Research Article

SOHAG JOURNAL OF SCIENCES

https://doi.org/10.21608/sjsci.2023.224819.1101

Petrophysical Parameters and Reservoir Evaluation from Well Log Analysis of Lam Member (Late Jurassic), Habban Oil Field, Marib-Shabwah (Sab'atayn) Basin, Yemen

Abdelbaset M. Abudeif[1,*], Ahmed E. Radwan[2], Nabeel A. S. Al-Azazi[3], Mohammed A. Mohammed[1], and Fahd M. Q. Basrada[1,2]

[1] *Geology Department, Faculty of Science, Sohag University, Sohag 82524, Egypt.*
[2] *Faculty of Geography and Geology, Institute of Geological Sciences, (Uniwersytet Jagielloński) Jagiellonian University in Krakow,31007, Poland.*
[3] *Department of Oil and Gas Engineering, Faculty of Oil and Minerals, Shabwah University, Shabwah, Yemen.*
**Email: a.abudeif@science.sohag.edu.eg*

Received: 10th August 2023, **Revised:** 9th September 2023, **Accepted:** 18th September 2023
Published online: 12th October 2023

Abstract: The present work aims to quantify the petrophysical parameters including shale content, effective porosity, and fluid saturations of the Late Jurassic Lam Member in the Habban oil field, Marib Shabwah Basin, Yemen, and also, to define the distribution and lateral connectivity of reservoir rocks which are frequently marked by severe lithological variation. The open-hole well log data from selected 5 wells, namely Habban 1A, Habban 8, Habban 11, Habban 14, and Habban 25 are used through computer software. The results revealed that the Lam Member rocks consist of an interbedded sequence of carbonate (limestone and dolomite) and claystone with intercalated sandstone. They are encountered in the study area with a relatively high thickness reaching up to 498 m. These rocks have reasonable effective porosity (12.2%), low shale content (14.9%), and high hydrocarbon saturation (70%) with maximum pay thicknesses reaching 40 m; accordingly, they are promising for future hydrocarbon exploration.
Keywords: Well logging analysis; Petrophysical parameters; Reservoir rocks; Lam Member; Habban Oilfield; Marib-Shabwah Basin.

1. Introduction

Yemen is situated on the southwestern margin of the Arabian Peninsula. Habban field is placed in the Saba'tayn sedimentary Basin (Marib-Al Jawf-Shabwah Basin) (Fig. 1). which is one of the most prolific Mesozoic hydrocarbon basins in western and central Yemen [1]. The Saba'tayn Basin is divided into three geographical sectors: Marib-Al Jawf, Shabwah, and Hajar [2]. In the late Jurassic and Early Cretaceous, a rift basin called the Saba'tayn Basin was created as a result of the Gondwanaland breakup, when the Indian Madagascar plate and the African Arabian plate separated apart [3,4]. As one of the Mesozoic rift basins, Saba'tayn Basin is known for its fast subsidence, phases of limited circulation, and the deposition of a range of sediments, such as organic-rich clay and shale, distal platform carbonates, delta sands, and cyclic terminal evaporates [5,6]. In the Red Sea coastal region of Yemen, the initial hydrocarbon prospecting began in 1961. Nevertheless, the initial commercial oil found in Yemen's Saba'tayn Basin at Block 18 marked the beginning of the oil era in that country's history in 1984. The first oil discovery in the Habban field within the boundaries of Block S-2 occurred in 1992 by the Canadian Occidental Oil Company. Thirteen of the 105 concession blocks that make up Yemen's concessions are oil-producing.

Among the operating blocks, five blocks (Block 18, Jannah 5, Damis S-1, West Ayad 4, and Al-Uqlah S-2) are situated in the Saba'tayn basin. The majority of Yemen's petroleum output comes from two rift basins: The Masila-Jeza basin in eastern Yemen and the Saba'tayn basin (Marib-Basin) in western Yemen. Most of these eastern and western basins are divided by the Mukalla structural height. The study area is part of block S-2 which is located in the northern branch of the Saba'tayn Basin (Marib-Shabwah Basin) in central Yemen.

Well logging analysis is one of the most popular methods for locating and assessing hydrocarbon reserves in open and cased holes. This technique is useful for determining reservoir petrophysical parameters including permeability, porosity, shale volume, and fluid saturation [7]. Also, it is important for estimating the lithology, thickness, and depth of productive zones and hydrocarbon reserves [8].

In the current study, detailed reservoir's petrophysical properties have been evaluated to assess Lam reservoir's hydrocarbon potential in the Habban field utilizing both geological and well logging data measured by Schlumberger Company including gamma ray (GR), caliper (CALI), shallow

resistivity (LLS), deep resistivity (LLD), bulk density (RHOB), sonic (DT), and neutron porosity (NPHI) from five wells, namely Habban 1A, Habban 8, Habban 11, Habban 14, and Habban 25 (Fig. 1).

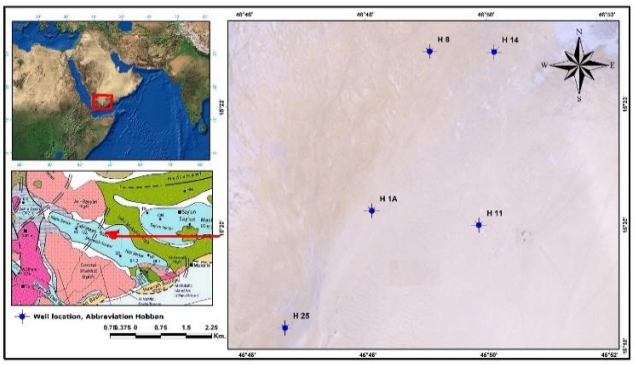

Figure 1: General maps showing the location of the area and of the studied wells in the Habban field (Marib-Shabwah Basin).

2. Geological Setting

Yemen, which is located in the southern part of the Arabian Peninsula, is geographically and geologically, in transition between Arabia and Africa. Two main tectonic events shaped Yemen's geological development. The first took place during the late Jurassic and Early Cretaceous, when the breakup of Gondwana (the separation of Africa and Arabia from India and Madagascar) led to the formation of the Mesozoic rift basins. The second significant tectonic event, which occurred in the Cenozoic (i.e., Late Oligocene-Pliocene), was associated with the opening of the Gulf of Aden and the Red Sea by the Arabian Plate breaking away from Africa and colliding with Eurasia [9]. Several scholars have researched Yemen's geology and stratigraphy e.g., [10], [11], [12], [13], [14], [15], [16], [17], [18], [6], [19], [20], [21] and [22]. The Saba'tayn Basin, which is 50 to 120 km broad and more than 450 km long, is one of Yemen's most productive Mesozoic rift basins. Al-Jawf, Marib, and Shabwah are among its sub-basins, which extend from northwest to southeast. A thick Mesozoic succession that averages up to 2,500 m in thickness dominates the stratigraphic section in Saba'tayn Basin. Along with Quaternary exposure, it reveals Jurassic to Cretaceous rock units resting on top of the pre-Cambrian basement rocks. The Saba'tayn Basin (Marib-Al Jawf-Shabwah Basin) is located between the Jahi-Mukalla High in the east and the Mahfid High in the west, In the south, the Jebel Al-Aswad Uplift separates The Saba'tayn Basin from the Cretaceous Balhaf Graben. [23] divided the Saba'tayn Basin's stratigraphic succession into three major tectono-stratigraphic megasequences: (a) a pre-rifting stage (Permian-Oxfordian/Kimmerdgian), (b) a syn-rifting stage (Kimmerdgian-Tithonian), and (c) a post-rifting stage (Early Cretaceous) (Fig. 2). The pre-rift stage consists of two periods: from the palaeozoic to the Triassic the area was uplift and eroded. During the early to late Jurassic, the general uplift continued with some intermittent phases of subsidence. Sandstone and conglomerates of the Kuhlan formation accumulated in an alluvial to fluvial and marine shoreline environment on top of the Proterozoic basement during Callovian and Oxfordian. In the late Oxfordian, the limestone of the Shuqra formation was formed on a shallow sea. The Shuqra limestone consists of argillaceous mud, wacke, and packstones.

Horsts and nested fault blocks are features of syn-rift sequences involving the Saba'tayn, Nyfa, and Madbi formations, which evolved throughout the Late Jurassic and Early Cretaceous periods [3]. The lower Meem and upper Lam are the two components that make up the Madbi formation [23]. Based on seismic interpretation, stratigraphic thicknesses range from 150 m to 200 m along the Basement elevations and up to 1800 m near the flanks. The lower Meem Member is mostly comprised of black calcareous shale with a few intercalations of bituminous limestone and turbiditic sandstone layers, whereas the upper Lam Member is a series of fine-grained limestone with thin bituminous shales, mudstone, and turbiditic sandstones deposited within a deep marine, partly restricted environment and is a prolific source rock in the Saba'tayn Basin (Fig. 3) [24]. Around the end of the syn-rift, decreasing subsidence rates combined with a low sea level resulted in the isolation of the basinal area (area of Block S-2) and the exposure and erosion of broad shelf areas (western of the Marib-Al Jwaf-Shabwah Basin). As a consequence, massive salt deposits of the Upper Tithonian Saba'tayn Formation were accumulated in the restricted parts of the basin, like in the block S-2 area [25]. The Saba'tayn Formation consists of thick halite strata together with interbeds of limestone, dolomite, and thin, partly bituminous shale and siltstone. Shallow marine limestones from the clastic rocks and Nayfa Formation from the Sa'ar Formation illustrate the transition to the early Cretaceous post-rift phase [25].

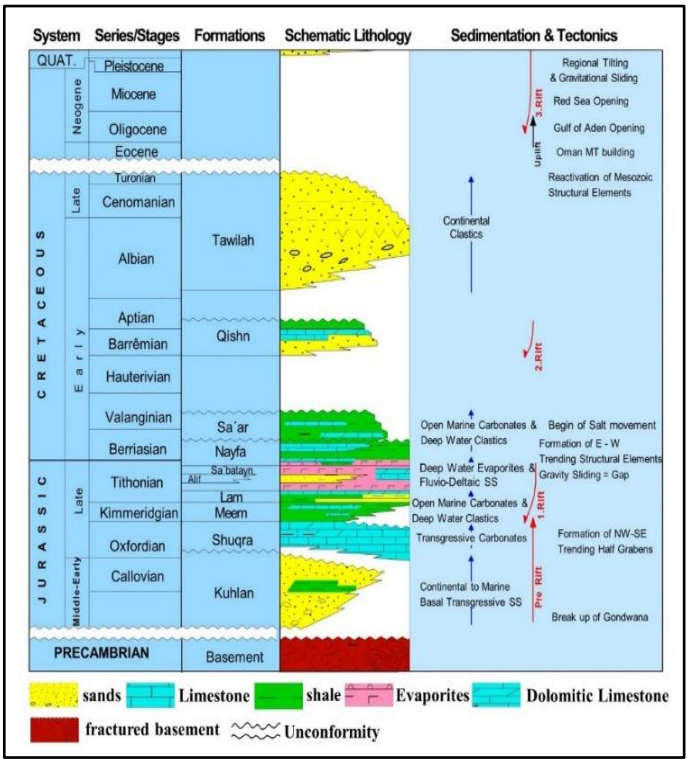

Figure 2: Lithostratigraphic and chronostratigraphic chart of Saba'tayn Basin (modified after [2,26].

The Sa'ar Formation is unconformably overlain by the Middle to Upper Cretaceous predominantly clastic Tawilah Group which consists of the older Qishn Formation and the Younger Tawilah Formation. The Qishn Formation (Hauterivian to Late Aptian-Early Albian) consists of a series of shallow marine carbonates and clastics. It is unconformably overlain by the Tawilah Formation deposited during the middle to Upper Cretaceous. the Tawilah Formation is a continental to marginal marine clastic deposits composed of poorly sorted sandstones and claystones that leveled off topography and stabilized the movement of Saba'tayn salt beneath. Within Block S2 isolated hills, like the Jebel Al Uqlah are built up by coarse-grained sandstones and conglomerates of the Tawilah Formation. The continental deposition continued through to the present with some Quaternary sands which are difficult to distinguish from the underlying Tawilah Formation.

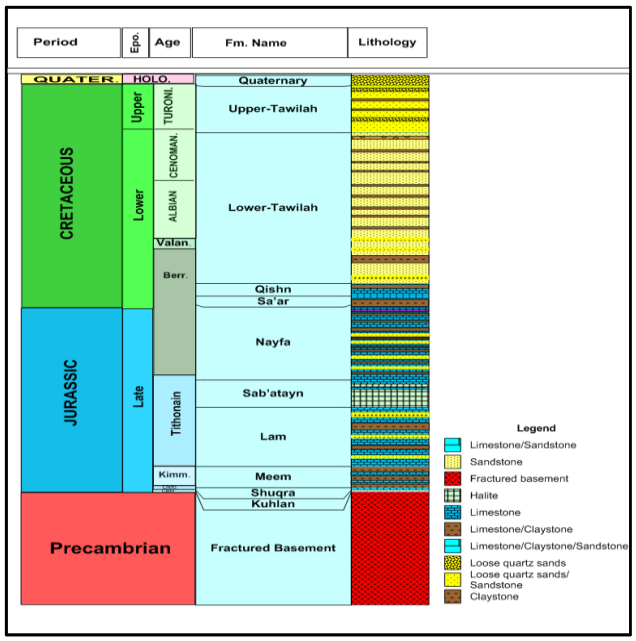

Figure 3: Lithostratigraphical succession of Habban oilfield, Sab'atayn Basin, Yemen (after [23,26]

3. Materials and methods

The conventional well log data from 5 wells (Habban 1A, Habban 8, Habban 11, Habban 14, and Habban 25) including gamma ray, density, neutron, sonic, resistivity (shallow and deep), and photoelectric factor (PEF) logs were interpreted to assess the hydrocarbon potentiality of Lam reservoir. A complete set of wireline log data for these five wells and drilling reports was acquired from the Open Market Value Company (OMV) as well as from the internal reports of the Petroleum Exploration and Production Authority-Yemen (PEPA). The Interactive Petrophysical (IP) Schlumberger software was used at the Petroleum Exploration and Production Authority (PEPA), Yemen, to conduct the qualitative and quantitative analyses using LAS files from the mentioned five given in Table 1 and (Fig. 1).

Table 1: List of well log tools in the study area.

Well name	Depth Intervals (m)	Logs
H 1A	2026 - 2233	BS-CALI-GR-LLD-LLS-DT-RHOB-NPHI
H 8	2026 -2384	BS-CALI-GR-LLD-LLS-DT-RHOB-NPHI
H 11	2037 - 2652	BS-CALI-GR-LLD-LLS-DT-RHOB-NPHI
H 14	2016 - 2308	BS-CALI-GR-LLD-LLS-DT-RHOB-NPHI
H 25	2147 - 2532	BS-CALI-GR-LLD-LLS-DT-RHOB-NPHI-PEF

4. Thickness Variations in the study area

The distribution and configuration of the Lam member late Jurassic sequence in the study area are delineated from the isopach contour map (Fig. 4), and correlation charts (Fig. 5), The isopach contour map (Fig. 4) depicting the thickness of the Lam Member (late Jurassic) in the research region reveals that the highest thickness is at Habban 11 well (615 m), while the thinnest layer reaches values of (207 m) at Haban 1A well.

In general, the Isopach map (Fig. 4) shows that the thickness distribution increases from the central area toward the southeastern while decreases from the northwestern parts toward the central area (lowest area) in the study area.

The lithostratigraphy of the sedimentary succession in the area for Lam Member in Habban oilfield (Late Jurassic) which was constructed along three profiles extending SW-NE, SE-NW, and W-SE based on the available subsurface borehole data (Fig. 5) (A - A¯), (B - B¯), and (C - C¯). Elevation values are tabulated in Table 1.

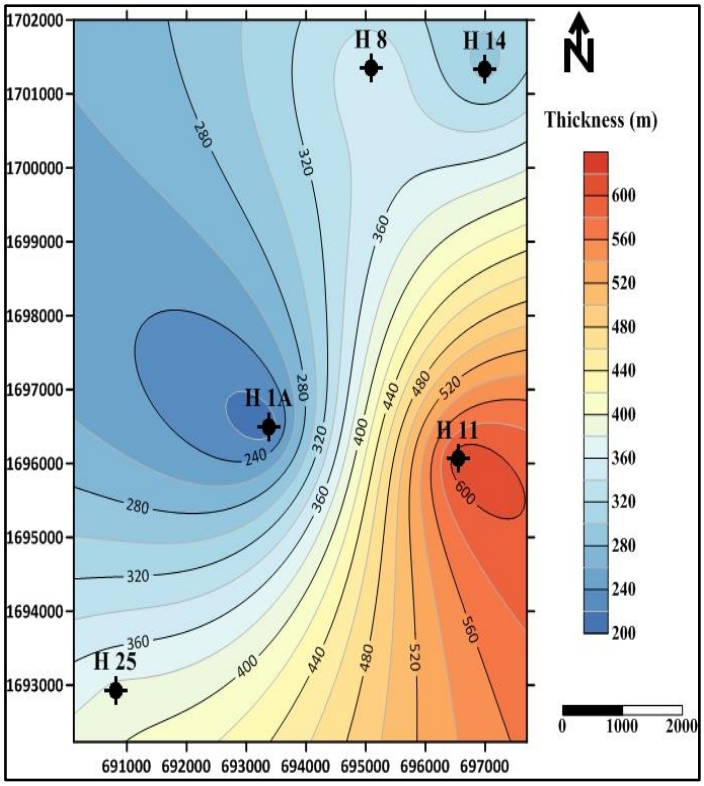

Figure 4: Isopach contour map of the Lam member in the study area.

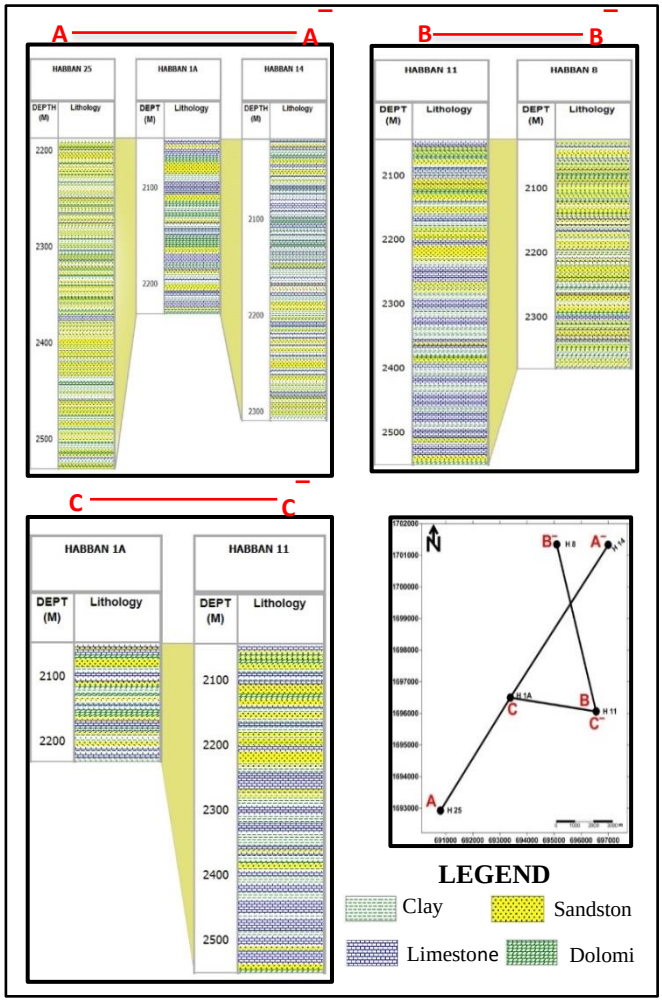

Figure 5: Correlation charts along profile (A - A¯) (SW-NE), (B - B¯) (SE-NW), and (C - C¯) (W-SE) showing the litho-stratigraphic rock units of the Lam member in the Sab'atayn Basin.

5. Well Log Analysis

The interpretation of the basic well logging data to evaluate the petrophysical parameters using the computer software IP (Interactive Petrophysics TM (2008) includes the following steps:

1- Determination and correction of the fluid resistivities (Rm, Rmf, and Rw). The formation water resistivity (Rw) is very important for the accurate determination of the fluid saturations. Using Pickett's Plot graphical technique, we calculated the Rw by measuring the resistivities of collected water samples [27]. This technique has the advantage of determining the cementation exponent (m) beside the accurate Rw values. (Fig. 6) reveals the porosity-resistivity cross-plot of the Lam Member Late Jurassic rocks in all wells. The determined formation water resistivity (Rw) values are 0.020, 0.035, 0.028, 0.029, and 0.022 ohm m in Habban 1A, Habban 8, Habban 11, Habban 14, and Habban 25 wells respectively, while the cementation factor (m) values are 2.2, 1.97, 2.07, 2.19 and 2.18 in Habban 1A, Habban 8, Habban 11, Habban 14, and Habban 25 wells respectively (Fig. 6). The high degree of cementation exponent m (1.97 to 2.2) refers to the highest values of the cohesion factor of carbonates due to diagenetic affinity and complex pore architecture.

2- Determination of the volume of shale content (Vsh) through the single and double shale indicators [27,28]. The Vsh used is the average of the gamma ray value and the lowest values deduced from the other tools. According to Schlumberger techniques for selecting the minimum value of shale volume, it was found that shale volume calculated from the gamma ray log is the minimum value of all the tools used to determine the volume of shale. This is principally due to its sensitive response to the radioactive materials normally concentrated in the shale rocks.

3- Determination of the formation porosity from the porosity logs (ΔT, ØN, and ρb).

$$\phi_S = \left(\frac{\Delta T_{log} - \Delta T_{ma}}{\Delta T_f - \Delta T_{ma}}\right) \times \frac{1}{C_P} \quad (1)$$

$$C_P = \frac{\Delta T_{sh}}{100} \times C \quad (2)$$

where: -

ØS is the porosity calculated from the sonic log (%).

ΔT_{log} is the sonic log (μ sec/ft).

ΔT_f is the acqustic travel time in the drilling fluid (μ sec/ft).

ΔT_{ma} is the acqustic travel time in the rock the matrix (μ sec/ft).

Cp is the compaction factor.

ΔT_{sh} is the specific transit time in adjacent shale (μ sec/ft).

C is the compaction coefficient (normally 1.0).

$$\phi_N = \phi_{log} - (V_{sh} * \phi_{Nsh}) \quad (3)$$

where: -

$Ø_N$ is the porosity calculated from the neutron log (%).

$Ø_{log}$ is the neutron log (%).

V_{sh} is the Shale volume.

N_{sh} is the Neutron shale value.

$$\phi_D = \frac{\rho_{ma} - \rho_b}{\rho_{ma} - \rho_f} \quad (4)$$

Where: -

ϕ_D is the porosity calculated from the density log (%).

P_b is the density log reading against a thick shale bed (gm/cc).

ρ_f is the density of fluid (gm/cc).

ρ_{ma} is the density of the matrix (gm/cc).

4- Determination of the water saturation by using the Indonesian [29] equation.

$$\frac{1}{\sqrt{R_t}} = \left[\sqrt{\frac{\phi^m}{a(R_w)}} + \frac{(V_{sh})^{(1-V_{sh}/2)}}{\sqrt{R_{sh}}}\right](S_w)^{(n/2)} \quad (5)$$

where: -

S_w is the water saturation in the uninvaded zone (%).

R_w is the formation of water resistivity (Ω.m).

R_t is the true resistivity of the uninvaded zone (Ω.m).

Ø is the formation porosity (%).

a is the tortuosity factor.
m is the cementation factor, equal to 2 in carbonates.
n is the saturation exponent which varies from 1.8 to 2.5.
R_{sh} is the resistivity of a thick shale unit.
V_{sh} is the Shale volume (%).

5- Determination of the hydrocarbon saturation (Sh) and Discrimination of hydrocarbons into the different types of gas or oil.

$$Sh = 1 - Sw \quad (6)$$
$$Shr = 1 - Sxo \quad (7)$$
$$Shm = Sh - Shr \quad (8)$$

where:
Sh is total hydrocarbon saturation.
Sxo is the water saturation n the uninvaded zone.
Sw is the water saturation.
Shr is the residual hydrocarbon saturation.
Shm is the movable hydrocarbon saturation.

6- Determination of the lithological components by using the simultaneous equations [30,31].

6. Results And Discussion

6.1. Litho-saturation crossplots

The crossplot for Lam Member illustrates the corrected log data and the litho-saturation in several tracks. The left-hand side tracks (from 1 to 3) display the studied units age. The next track (number 4), displays the depth. Track (number 5) includes the caliper log readings, the bit size, the gamma-ray log, the washout and the mud cake. The next track (number 6), displays the corrected density log, neutron log, and photoelectric factor log. The track (number 7), displays the corrected resistivity logs. The track (number 8), displays the sonic log. The following tracks (from 9 to 13) represent across the well in a vertical direction the well log deduced lithology, petrophysical, and fluid characteristics of the examined intervals. The characteristics, from left to right, include the values of total porosity (PHIT) secondary porosity(PHISEC), effective porosity (PHIE), the lithofacies analysis (clay, limestone, dolomite, and sand), the fluids saturation curves (hydrocarbon and water). and finally the pay flag of the Lam Member. In Habban 1A, Habban 8, Habban 11, Habban 14, and Habban 25. For illustrations the corrected log data and litho-saturation results of Habban 8 and Habban 14 well are shown in (Figs. 7 and 8), respectively.

Depending on the well logging analysis, the vertical distribution of petrophysical parameters can be used to evaluate the Lam Member. To identify zones for prospective testing in the future, this assessment of reservoir potential will be helpful.

Table 2: Average petrophysical parameters of Lam Member for all wells in the study area.

Well name	Top	Bottom	Gross	Net	N/G	PHIE%	Vsh%	SW%	SH%
H 1A	2050	2233	183	18.75	0.102	11.5	20.3	43.2	56.8
H 8	2027.3	2381	353.7	34.25	0.097	11.6	22.7	41.3	58.7
H 11	2050	2548	498	27.5	0.055	12.2	19.1	41.2	58.8
H 14	2016	2309	293	39.73	0.136	12	23.3	31.1	68.9
H 25	2189	2532	343	11.77	0.034	10.8	14.9	40.2	59.8

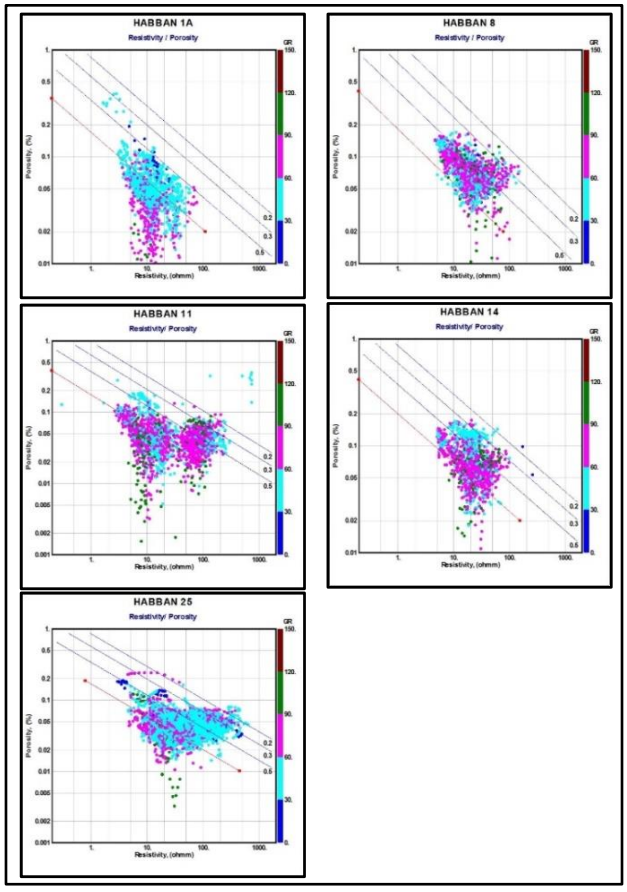

Figure 6: Pickett's plots of the Lam member in the studied wells.

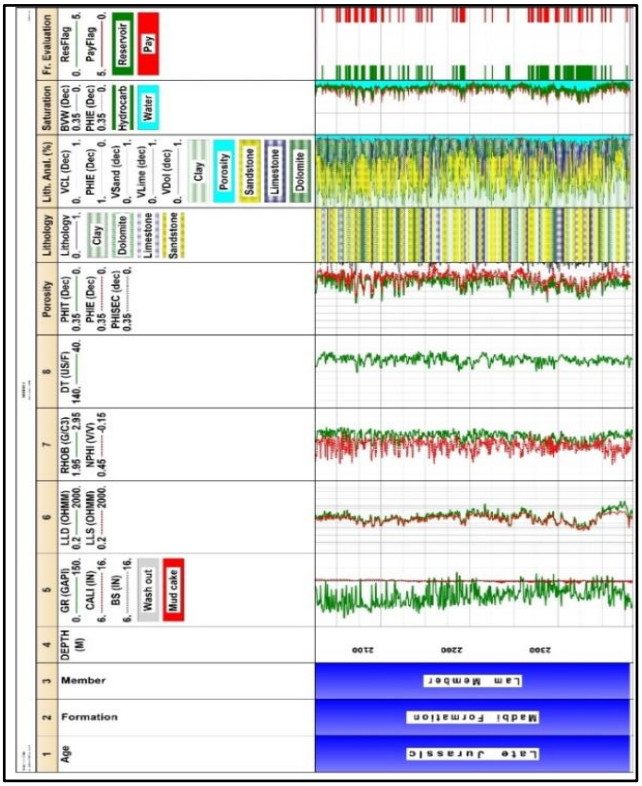

Figure 7 The litho-saturation cross-plot illustrating vertical variations in the petrophysical characteristics of the Lam member by Schlumberger IP (Interactive Petrophysics) software for Habban 8 well.

6.2. Distribution of petrophysical properties

6.2.1. Volume of Shale Distribution Map

The volume of shale contour map of the Lam Member (Fig. 9A) displays a typical pattern of distribution with an overall increasing trend in the north and north-east of the study area, with maximum values of (23.3%) at the Habban 14 well and minimum values of (14.9%) at the Habban 25 well in the south-west.

6.2.2. Effective Porosity Distribution Map

Effective porosity (Øe) is the most significant petrophysical feature, which represents the capacity of the Lam Member (Late Jurassic) reservoir. It is the proportion of the total volume of reservoir rock comprised of empty space linked by flow channels. A gradual increase in the average effective of porosity from the southwestern to the northeastern region of the study area, which has the greatest value (12.2%) at Habban 11 well, is shown on the effective porosity distribution map of the Lam Member (Fig. 9B). The research area's effective porosity diminishes towards the southwest. The lowest value (10.8%) is shown at Habban 25 well.

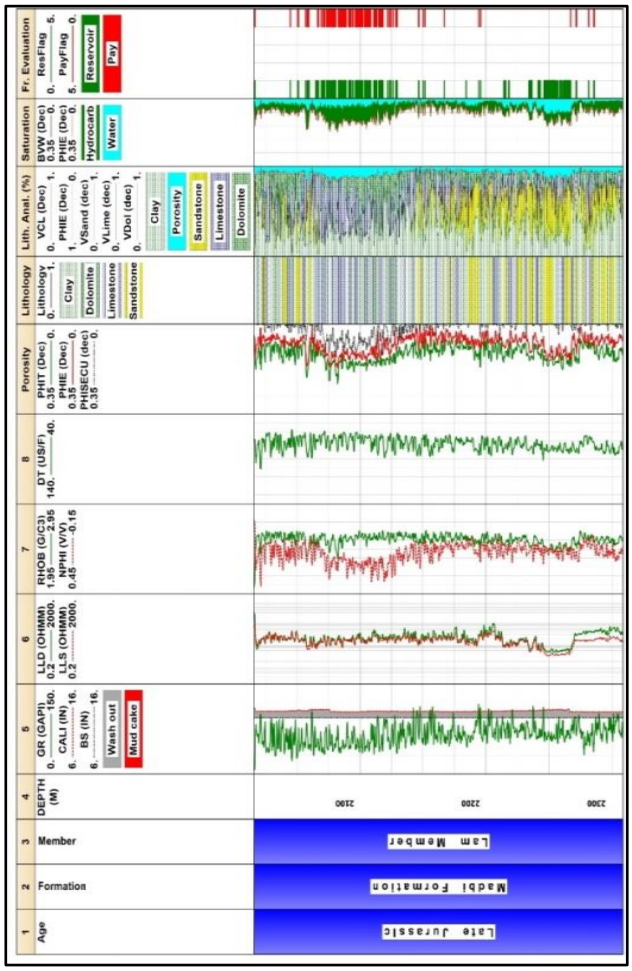

Figure 7: The litho-saturation cross-plot illustrating vertical variations in the petrophysical characteristics of the Lam member by Schlumberger IP (Interactive Petrophysics) software for Habban 14 well.

6.2.3. Hydrocarbon Saturation Distribution Map

In the studied region, the hydrocarbon saturation map of the Lam Member (Fig. 9C) records a maximum value of (68.9%) at the Habban 14 well and a minimum value of (56.8%) at the Habban 1A well, with increases toward the northeastern sections and declines in the middle.

6.2.4. Water Saturation Distribution Map

The water saturation distribution map of Lam Member (Fig. 9D) shows variation in water saturation values least value of (31.1 %) at the Habban 14 well to the highest value of (43.2 %) at the Habban 1A well. In general, the research area's water saturation distribution rises from the center toward the northeast.

6.2.5. Net Thickness and Net to Gross Thickness Ratios Distribution

The net thickness distribution map of Lam Member (Fig. 10A) reveals variation in net thickness values, from the lowest value of 11.77 m at the Habban 25 well to the highest value of 39.73 m at the Habban 14 well. Generally, the net thickness distribution increases towards the northeastern sections of the study area, while it declines towards the southwest sections of the study area. By contrast, net to gross thickness ratios distribution map of the Lam Member (Fig. 10B) shows a similar distribution pattern for the net thickness distribution map of the Lam Member, the minimum net-to-gross thickness ratios recorded a value of 0.034 at Habban 25 well, while the maximum value of 0.136 at Habban 25 well. Generally, the net-to-gross thickness ratio distribution increases towards the northeastern parts, while decreasing towards the southwest parts of the study area. The distribution pattern points to the northeastern parts of the Lam Member as promising sites for hydrocarbon exploration.

6.3. The hydrocarbon potentialities of the study area

The potentialities of the hydrocarbon in the study area can be predicted by integrating the lithological, petrophysical, fluid parameters, and hydrocarbon generation factors affecting the investigated area. through comprehensive analyses. Consequently, a lease map is constructed for the studied Lam member (Fig. 11). based on pay zone thickness, hydrocarbon saturation, and some reservoir petrophysical factors like effective porosity and shale volume. This map is helpful for future exploration plans and the development of the study area.

6.3.1. Lease map of the Lam Member

The lease map of Lam Member (Fig. 9D) indicates that the petrophysical characterization of Lam Member (Late Jurassic) is a good reservoir in the northeastern part of the study area, where there is a remarkable decrease in the shale content reflecting the increase of effective porosity and giving rise to the opportunity to increase the accumulation of hydrocarbon saturation. These areas are areas of great productivity and reveal promising sites for future hydrocarbon exploration. These sites have hydrocarbon saturations between (57%) to (69%), shale contents between (15%) to (23%), effective porosity between (10%) to(12%) and maximum pay thicknesses ranging from 12 m to 40 m.

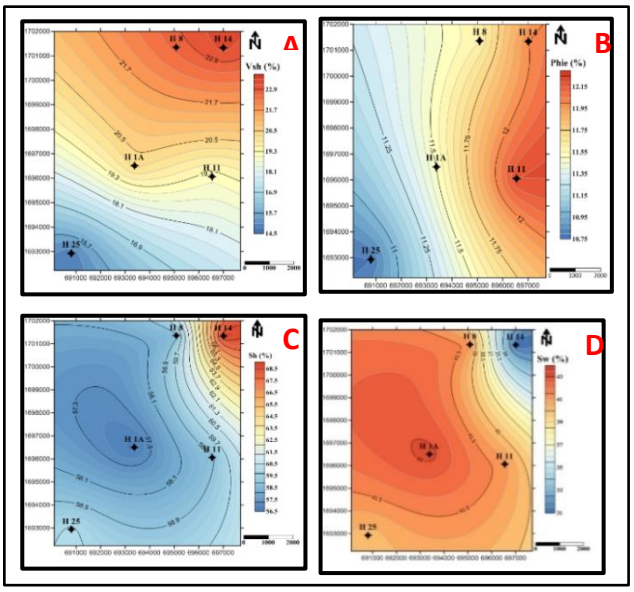

Figure 9: (A) Shale volume contour map, (B) Effective porosity contour map, (C) Hydrocarbon saturation contour map and (D) Water saturation contour map of the Lam member.

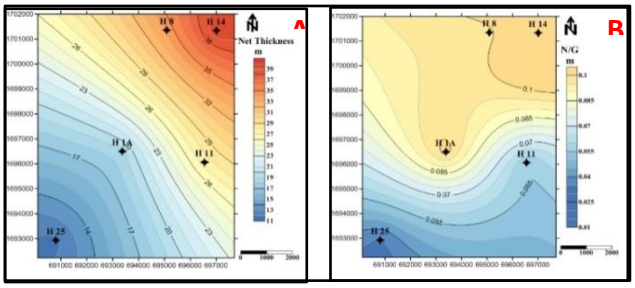

Figure 10: (A) Net Thickness contour map, (B) Net thickness to gross thickness ratios contour map of the Lam member.

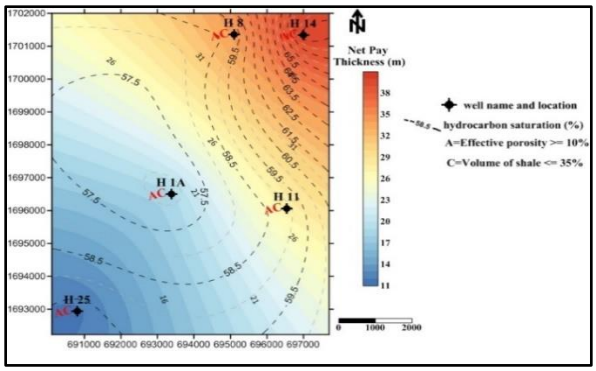

Figure 11: Lease map illustrating the net pay thickness (colored area), hydrocarbon saturation (dashed lines) and some parameters (Effective porosity, volume of the shale) of the Lam member.

7. Conclusions

By the integrated well log petrophysical analysis, subsurface geology, and formation evaluation of Lam Member (Late Jurassic) at the five wells in Habban Oil Field the following conclusions could be outlined:

1- The Lam Member consists of an interbedded sequence of carbonate (limestone and dolomite) and claystone with intercalated sandstone.

2- The Late Jurassic rocks of Lam Member are encountered in the study area with a high thickness reaching up to 498 m.

The shale content in Lam Member increases from the southwestern to the north and northeastern parts of the study area. The abundant shale content in the Lam Member section varies from (14.9%) to (23.3%).

The average effective porosity of Lam Member rocks in the studied five wells is generally moderate and ranges from (10.8%) to (12.2%).

The hydrocarbon saturation of Lam Member increases towards the northeastern parts, whereas it decreases in the middle of the study area recording the highest value of (68.9%) towards the northeastern parts These results lead to consider Lam Member as promising for future hydrocarbon exploration in Habban Oil Field.

Acknowledgment

The authors would like to express our appreciation to the Petroleum Exploration and Production Authority (PEPA) of the Republic of Yemen and the Exploration and Production Company (OMV) for providing well data and log data upon which this study was based in the Habban oilfield.

CRediT authorship contribution statement:

Conceptualization, Abdelbaset. M. Abudeif, Nabeel A. S. Al-Azazi, Ahmed E. Radwan and Mohammed A. Mohammed; methodology, Abdelbaset. M. Abudeif, Nabeel A. S. Al-Azazi and Fahd. M. Q. Basrada; software, Abdelbaset. M. Abudeif, Nabeel A. S. Al-Azazi, Mohammed A. Mohammed and Fahd. M. Q. Basrada; validation, bdelbaset. M. Abudeif, Nabeel A. S. Al-Azazi, and Ahmed E. Radwan; formal analysis, Ahmed E. Radwan, Nabeel A. S. Al-Azazi and Fahd. M. Q. Basrada; investigation, Abdelbaset. M. Abudeif, Nabeel A. S. Al-Azazi, Mohammed A. Mohammed, Ahmed E. Radwan and Fahd. M. Q. Basrada; resources, Nabeel A. S. Al-Azazi and Fahd. M. Q. Basrada; data curation, Abdelbaset. M. Abudeif, Nabeel A. S. Al-Azazi, Mohammed A. Mohammed, Ahmed E. Radwan and Fahd. M. Q. Basrada; writing—original draft preparation, Abdelbaset. M. Abudeif, Nabeel A. S. Al-Azazi and Fahd. M. Q. Basrada; writing—review and editing, Abdelbaset. M. Abudeif, Nabeel A. S. Al-Azazi; visualization, Abdelbaset. M. Abudeif, Nabeel A. S. Al-Azazi and Fahd. M. Q. Basrada; supervision, Abdelbaset. M. Abudeif, Nabeel A. S. Al-Azazi, Ahmed E. Radwan and Mohammed A. Mohammed; project administration, Nabeel A. S. Al-Azazi and Fahd. M. Q. Basrada; funding acquisition, Nabeel A. S. Al-Azazi and Fahd. M. Q. Basrada. All authors have read and agreed to the published version of the manuscript.

Data availability statement

The data used to support the findings of this study are available from the corresponding author upon request.

Declaration of competing interest

The authors declare that they have no known competing financial interests or personal relationships that could have appeared to influence the work reported in this paper.

References

[1] T.S. Ahlbrandt, *United States Geological Survey Bulletin*, (2002) 33.
[2] Z. Beydoun, M. As-Saruri, and R. Baraba, *Revue de l'Institut Français du Pétrole*, 51 (1996) 763-775.
[3] P. Redfern and J.A. Jones, *Basin Research*, 7 (1995) 337-356.
[4] Z.R. Beydoun, *Marine and Petroleum Geology*, 14 (1997) 617-629.
[5] I.D. Maycock, *Assoc. Pet. Geol., Bull.; (United States)*, 70 (1986) 930.
[6] A. Taheri, et al., *Middle East Well Eval Rev Schlumberger*, 12 (1992) 12-29.
[7] Schlumberger, *Schlumberger Limited: New York*, (1974) 116.
[8] G.A.a.D. Krygowski, *The American Association of Petroleum Geologists: Tulsa, Oklahoma*, (2004) 244.
[9] I. Csato and P. January, *AAPG Annual Convention, Dallas*, (2004) 1-6.
[10] Z.R. Beydoun, *HMSO: London*, (1964) 107.
[11] R.W. Powers, et al., *Geological Survey U. S.*, (1966) 1–147.
[12] Z.R. Beydoun and J. Greenwood, Aden protectorate and dhufar, internatiomal union of Geological Sciences, Comission on Stratigraphy, (1968) 126.
[13] M.W.H. Clarke, *Journal of Petroleum Geology*, 11 (1988) 5-60.
[14] Z. Beydoun, *Journal of Petroleum Geology*, 12 (1989) 125-144.
[15] F. Haitham and A. Nani, *Journal of Petroleum Geology*, 13 (1990) 211-220.
[16] S. Paul, *Geological Society, London, Special Publications*, 50 (1990) 329-339.
[17] G. Hughes and Z. Beydoun, *Journal of Petroleum Geology*, 15 (1992) 135-156.
[18] W. Bott, et al., *Journal of Petroleum Geology*, 15 (1992) 211-243.
[19] Z. Beydoun, M. Bamahmoud, and A. Nani, *Marine and Petroleum Geology*, 10 (1993) 364-372.
[20] N. Al-Azazi, *Unpublished M. Sc. Thesis, Menoufiya Univ., Egypt*, (2010) 236.
[21] N.A. Al-Azazi, *Faculty of Science, Ain Shams University*, (2016) 257.
[22] M. Albaroot, *Unpublished PhD thesis, Aligarh Muslim University, India*, (2017).
[23] Z.R. Beydoun, *IUGS and Ministry of Oil and Mineral Resources, Republic of Yemen*, (1998) 245.
[24] A. Alaug, et al., *Iranian Journal of Earth Science*s, 3 (2011) 134-152.
[25] T.R. Seaborne, *Marine and Petroleum Geology*, 13 (1996) 963-972.
[26] M.A. As-Saruri, R. Sorkhabi, and R. Baraba, *Springer*, (2013) 361-373.
[27] Schlumberger, *Services Techniques Schlumberger*, (1972) 45-67.
[28] A. Dresser, *Houston, Texas*, (1983) 149.
[29] J. Leveaux and A. Poupon, *The Log Analyst*, 12 (1971) 3-8.
[30] J.A. Burke, R.L. Campbell, and A.W. Schmidt, The litho-porosity cross plot a method of determining rock characteristics for computation of log data, SPE Illinois Basin Regional Metting, OnePetro, (1969) 25-43.
[31] M.H. Harris and R. McCammon, *AIME, Denver, Colorado, U. S. A.*, (1969) 239-248.